ACS APPLIED MATERIALS & INTERFACES

Research Article

www.acsami.org

Preparation and Mechanism of Cu-Decorated TiO_2–ZrO_2 Films Showing Accelerated Bacterial Inactivation

Sami Rtimi,[†] Cesar Pulgarin,[†] Rosendo Sanjines,[‡] Victor Nadtochenko,[§] Jean-Claude Lavanchy,[∥] and John Kiwi*[,†]

[†]Ecole Polytechnique Fédérale de Lausanne, EPFL-SB-ISIC-GPAO, Station 6, CH-1015, Lausanne, Switzerland

[‡]Ecole Polytechnique Fédérale de Lausanne, EPFL-SB-IPMC-LPCM, CH-1015 Lausanne, Station 3, Switzerland

[§]Institute of Chemical Physics RAS, Kosigin Str. 4, Moscow, 19991, Russia

[∥]Université de Lausanne, IMG, Centre d'Analyse Minerale, Bat. Anthropole, CH-1015, Lausanne, Switzerland

ABSTRACT: Antibacterial robust, uniform TiO_2–ZrO_2 films on polyester (PES) under low intensity sunlight irradiation made up by equal amounts of TiO_2 and ZrO_2 exhibited a much higher bacterial inactivation kinetics compared to pure TiO_2 or ZrO_2. The TiO_2–ZrO_2 matrix was found to introduce a drastic increase in the Cu-dopant promoter enhancing bacterial inactivation compared to Cu sputtered in the same amount on PES. Furthermore, the bacterial inactivation was accelerated by a factor close to three, by Cu– on TiO_2–ZrO_2 at extremely low levels ~0.01%. Evidence is presented by X-ray photoelectron spectroscopy for redox catalysis taking place during bacterial inactivation. The TiO_2–ZrO_2–Cu band gap is estimated and the film properties were fully characterized. Evidence is provided for the photogenerated radicals intervening in the bacterial inactivation. The photoinduced TiO_2–ZrO_2–Cu interfacial charge transfer is discussed in term of the electronic band positions of the binary oxide and the Cu TiO_2 intragap state

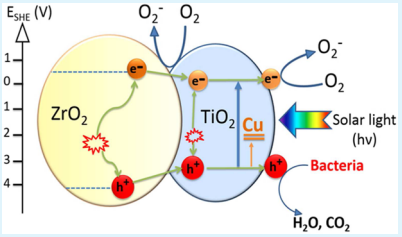

KEYWORDS: *TiO_2–ZrO_2 film composites, photocatalysis, Cu-doping, band gap of cosputtered TiO_2–ZrO_2–Cu, bacterial inactivation, redox catalysis*

INTRODUCTION

Bacteria and other pathogens induce infections that can be reduced/eliminated by surfaces presenting photocatalytic antibacterial properties.[1−3] This leads to hospital-acquired infections (HAI) with and associated high health care costs[3−6] and a need for antibiotics. But antibiotics administered for long times lead to bacterial resistance. Healthcare associated infections (HCAI) have become more frequent in the past decade with concomitant higher cost treatments.[7] There is a need to develop resistant noncorrosive materials that present fast bacterial reduction kinetics, long-term operational lifetime, and acceptable biocompatibility.[8−10]

Recent research has explored the use of binary metal oxides, doped or not, for a variety of industrially processes. This study addresses the synthesis of binary oxides and their evaluation in bacterial/biofilm formation. We specifically address the sputtering of uniform, adhesive, photoresistant nanoparticulate TiO_2–ZrO_2 and TiO_2–ZrO_2–Cu films and their performance in bacterial inactivation under low intensity sunlight. Until now, TiO_2–ZrO_2 films prepared by sol–gel methods and used as powders and annealed at a few hundred degrees have been reported for their use in industrial processes.[11,12] Sol–gel coatings in general are not reproducible or mechanically stable and show only a low adhesion to the substrate.[13] Cu has been widely reported as an effective bactericide. In this study, we address the effect of Cu added in extremely small concentrations to TiO_2–ZrO_2 polyester (PES). TiO_2–ZrO_2 films have been recently reported[14,15] as a resistant noncorrosive industrial catalyst but not investigated for its use in bacterial inactivation.

Cu-coatings on textiles at relatively low temperatures on low thermal resistant fabrics have been recently reported in the literature.[16−19] Many research groups have reported recently antibacterial Cu- and TiO_2-coated glass and polymer films, depositing the metal and oxides mainly by chemical vapor deposition (CVD).[20−24] Kelly et al. have reported the preparation of films by sputtering reducing *Escherichia coli* cell viability.[25,26]

The objective of the present work is to investigate the photocatalytic use of the TiO_2–ZrO_2–Cu films inactivating bacteria. These compounds have been reported in powder form[11−15] and films,[14,15] addressing their usefulness as catalysts, electronic devices, and in optical applications. We report in this study: (1) the preparation of Cu-doped TiO_2–ZrO_2 by magnetron sputtering (MS); (2) the *E. coli* bacterial inactivation kinetics of these films under low intensity sunlight irradiation; (3) the surface microstructure and its correlation with antibacterial reactivity; (4) the photoinduced interfacial charge transfer (IFCT) mechanism between TiO_2 and ZrO_2; and (5) the role of the Cu on the TiO_2–ZrO_2 film In the ppb

Received: March 11, 2015
Accepted: May 29, 2015
Published: May 29, 2015

ACS Publications © 2015 American Chemical Society

DOI: 10.1021/acsami.5b02168
ACS Appl. Mater. Interfaces 2015, 7, 12832−12839

range as a metabolizable, noncytotoxic species[27] inactivating bacteria through an oligodynamic effect[28] due to its binding the S, N, and COO^- cell wall electron donor negative groups.

EXPERIMENTAL SECTION

Sputtering of TiO_2–ZrO_2 on PES and X-ray Fluorescence Determination of the Films Content. Thin Ti and Zr films were sputtered on PES by magnetron sputtering in a reactive oxygen atmosphere using 50/50 mixed targets of Ti and Zr from Kurt J. Lesker Co, (Hastings, U.K.). The substrate-to-target distance was 10 cm, and the targets were 2 in. in diameter. Cu doping was subsequently carried out by sputtering Cu on the TiO_2–ZrO_2 films for times ≤10s.

The PES used was Dacron, type 54 spun, plain weave ISO 105-F04 (EMPA) used for color fastness determinations. The nominal thickness calibration of the TiO_2–ZrO_2 films was carried out on Si-wafers with a profilometer (Alphastep500, TENCOR) and presented an error margin of ±10%. The results are shown in Table 1. The TiO_2, ZrO_2, and Cu content in the samples were evaluated by X-ray fluorescence in a PANalytical PW 2400 unit as a function of the sputtering time. When cosputtering TiO_2 and ZrO_2, a redistribution of the Ti–Zr-oxides apparently occurs when the binary oxide TiO_2–ZrO_2 is formed in the topmost PES layers. This is a possible reason for the decease of the TiO_2 and ZrO_2 content when cosputtering for longer times (Table 1)

Table 1. Thickness Calibration of TiO_2–ZrO_2 Sputtered for 8, 10, and 12 min and TiO_2 ZrO_2/Cu (8 min/10s) on Si-Wafer

	thickness (nm)	atomic layers
TiO_2–ZrO_2 (8 min)	100	500
TiO_2–ZrO_2 (10 min)	130	650
TiO_2–ZrO_2 (12 min)	145	725
TiO_2–ZrO_2/Cu (8 min/10s)	120	600

Bacterial Inactivation of *E. coli* on PES-Sputtered Samples and Irradiation Procedures. The samples of *E. coli* K12 was obtained from the Deutsche Sammlung von Mikro-organismen and Zellkulturen GmbH (DSMZ) ATCC23716, Braunschweig, Germany to test the sample bacterial reduction activity. PES was sterilized by autoclaving at 121 °C for 2 h. Then, 20 μL bacterial culture aliquots with a concentration ~10^6 CFU mL^{-1} in NaCl/KCl were placed on unsputtered (control samples) and the sputtered PES fabrics. The samples were placed on Petri dishes and covered with a lid to prevent evaporation. At preselected times, the samples were transferred into a sterile 2 mL Eppendorf tube containing 1 mL autoclaved NaCl/KCl saline solution. These solutions were subsequently mixed thoroughly using a Vortex for 3 min. Serial dilutions were made in NaCl/KCl solution taking a 100 μL sample and then pipetting the aliquot onto a nutrient agar plate for subsequent bacterial counting by the standard plate method. These agar plates were incubated, lid down, at 37 °C for 24 h before the colonies were counted. Triplicate runs were carried for the bacterial CFU/mL^{-1} determination reported in this study. To verify that no regrowth of *E. coli* occurs after the first bacterial reduction cycle, the nanoparticle film was incubated again on an agar Petri dish at 37 °C for 24 h. No bacterial regrowth was observed. The sputtered samples were irradiated with the Xe-400W lamp in the Suntest solar simulator CPS (Atlas GmbH, Hanau, Germany) with a light dose of 50 mW/cm^2 (~0.8×10^{16} photons/s), and a cutoff filter was added in the Suntest cavity to filter the light <310 nm.

Fluorescence Stereomicroscopy, Diffuse Reflectance Spectroscopy (DRS), and Composite Band Gap (bg) Determination. The fluorescence stereomicroscopy was carried out on samples inoculated with 10^8 CFU of *E. coli* and incubated for 2 h in a humidification chamber. This method uses a fluorochrome-based staining procedure from Filmtracer LIVE/DEAD Biofilm Viability Kit (Molecular Probes, Invitrogen). The kit contains a combination of the SYTO 9 green fluorescent nucleic acid stain and propidium iodide fluoro-chromes for the staining of live and dead cells, respectively. The sample fluorescence was monitored in a fluorescence stereomicroscope (Leica MZ16 FA, Leica Microsystems GmbH Wetzlar, Germany), and the images were processed using the LAS v.1.7.0 build 1240 software from Leica Microsystems CMS GmbH. Adhesion of bacteria to the sputtered polyester was allowed for 2 min before the sample was washed with sterile Milli-Q water to remove nonadherent bacteria. Images were monitored to show both statements (live, dead, or both) of bacteria on the samples.

DRS was carried out in a PerkinElmer Lambda 900 UV–vis-NIR spectrometer within the wavelength range of 200–800 nm. The rough UV–vis reflectance data cannot be used directly to assess the optical absorption of the samples because of the large scattering contribution of the PES fabric to the DRS spectra. Normally, a weak dependence is assumed for the scattering coefficient S on the wavelength. The spectra obtained by DRS are plotted in Kubelka–Munk (KM) units. The band gap plots for TiO_2–ZrO_2 and TiO_2–ZrO_2-Cu were carried out following the Tauc's method.[30] The energy dependence of the semiconductor absorption relates to the adsorption coefficient of the composite semiconductor band gap (Eg).

X-ray Diffraction (XRD) and X-ray Photoelectron Spectroscopy (XPS) of Sputtered Uniform Films. The crystalline structures of the samples reported in this study were investigated by X-ray diffraction by means of an INEL Model XRG instrument 3.5KW power with a detector to register θ peaks from 2° to 120°.

An AXIS NOVA photoelectron spectrometer (Kratos Analytical, Manchester, U.K.) equipped with monochromatic Al Kα ($h\nu$ = 1486.6 eV) anode was used during the study. The carbon C 1s position at 284.6 eV was the reference used to correct the charging effect. The XPS spectra were deconvoluted by means of the software CasaXPS-Vision 2, Kratos Analytical).

Monitoring of Oxidative Radicals on TiO_2–ZrO_2–Cu PES Using the Fluorescence Technique. The detection of the oxidative species (mainly OH-radicals) was carried out according to Hashimoto et al.[31] Terephthalic acid 99% was obtained from Across and the NaOH 98% was from Sigma-Aldrich. A sample of 4 cm^2 of TiO_2 coated fabric was immersed in a solution made of terephthalic acid at 0.4 mM dissolved in a 4 mM NaOH solution. After each irradiation, the solution was transferred in a quartz cell and the fluorescence spectra of 2-hydroxyterephthalic acid generated by the reaction of terephthalic acid with the OH containing compound were measured on a PerkinElmer LS-50B fluorescence spectrometer. The spectra were recorded between 400 and 500 nm (scan rate: 100 nm/min) under an excitation at 315 nm.

The determination of other oxidative species leading to *E. coli* inactivation was carried by inoculating TiO_2–ZrO_2/Cu surfaces with *E. coli* in the presence or absence of ionic chelators or ROS quenchers. Aliquots of the bacterial suspension were suspended on TiO_2–ZrO_2–Cu PES in either phosphate-buffered saline (PBS) alone (control) or PBS supplemented with a chelating agent or ROS quencher (Sigma, U.K.) adding a 20 μL of bacteria (~10^7 CFU/ml) sample. Ethylenediamine-tetra-acetic acid sodium (EDTA-2Na) was added to the photocatalyst as hole (h+) scavenger. Dimethyl sulfoxide (DMSO) was used as (OH°) scavenger and finally and superoxide dismutase (SOD) was the HO_2° scavenger.

RESULTS AND DISCUSSION

Coating Thickness and X-ray Fluorescence (XRF) Determination. Thicknesses of the coatings for TiO_2–ZrO_2 and TiO_2–ZrO_2–Cu are shown in Table 1 as a function of the sputtering time. TiO_2–ZrO_2 was sputtered from one single target. Because one atomic layer comprises 10^{15} atom/cm^2, the atomic layers were deposited at a rate 0.8×10^{15} atoms/cm^2-s. Table 1 shows a coating thickness of 120 nm or about 600 layers[29] for the sample leading the fastest bacterial inactivation kinetics. The TiO_2–ZrO_2–Cu films sputtered for 8 min were

DOI: 10.1021/acsami.5b02168
ACS Appl. Mater. Interfaces 2015, 7, 12832–12839

then Cu-sputtered for 5s and attained the content of 0.47% TiO_2 and 0.47% ZrO_2 weight/weight PES, as shown in Table 2.

Table 2. XRF Determination of Weight % of TiO_2, ZrO_2 and Cu Sputtered on Polyester (PES)

	weight % TiO_2/ wt PES	weight % ZrO_2/ wt PES	Weight % Cu/ wt PES
TiO_2–ZrO_2 (6 min)	0.42	0.54	
TiO_2–ZrO_2 (8 min)	0.47	0.47	
TiO_2–ZrO_2 (12 min)	0.44	0.52	
TiO_2–ZrO_2/Cu (8 min/5 s)	0.47	0.47	0.01
TiO_2–ZrO_2/Cu (8 min/10 s)	0.45	0.48	0.02

***E. coli* Bacterial Reduction under Low Intensity Sunlight Irradiation on Binary Oxide Catalysts.** In the dark, no bacterial inactivation was observed when using the TiO_2, ZrO_2, and TiO_2–ZrO_2. TiO_2 (bg 3.2 eV)[32] and ZrO_2 (bg 4.5)[33] have been reported to be active in bacterial inactivation. TiO_2–ZrO_2 materials have been reported to accelerate catalytic oxidation of ethylene compared to either component and other organics due to surface OH groups.[33,34] Binary ZrO_2–TiO_2 shows higher acidity compared to each of the component oxides and a significant lower amount of dissociated OH surface groups.[35,44] Synergy was reported for the TiO_2–SiO_2 binary oxide[11] prepared by sol–gel and seems to be improving the generation of highly oxidative radicals.[9] Furthermore, Cu forms complexes with various Lewis bases, increasing its adsorption capacity in a variety of catalytic processes.[36] Figure 1a shows the bacterial reduction by TiO_2–ZrO_2 at different deposition times on PES. A sputtering time of 8 min seems to induce the faster bacterial inactivation. Thicker coatings applied due to longer sputtering times led to coatings with a lower surface charge due to inward bulk diffusion as well as the detrimental effect particles with larger sizes undergoing agglomeration.[46]

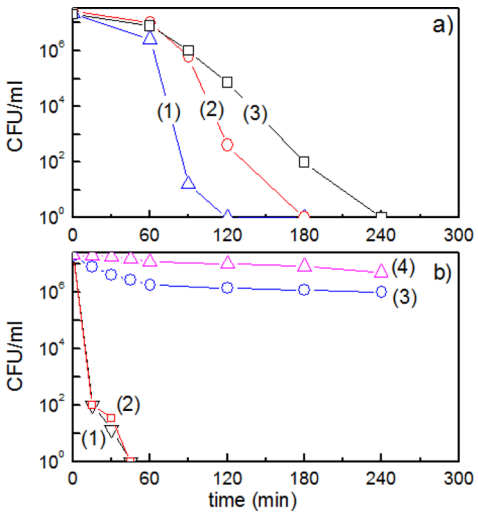

Figure 1. (a) *E. coli* inactivation on TiO_2–ZrO_2 PES samples sputtered for (1) 8 min, (2) 10 min, and (3) 12 min under low intensity solar light irradiation (50 mW/cm^2). (b, 1 and 2) *E. coli* inactivation on TiO_2–ZrO_2 samples cosputtered for 8 min followed by Cu-sputtering for 5s and 10s; (3 and 4) Cu sputtered for 5 and 10s on PES as control experiment under low intensity solar light irradiation (50 mW/cm^2).

Figure 1b shows that Cu-doping accelerated the bacteria kinetics 3-fold at Cu 0.01–0.02% w/w PES. Cu-doped samples reduce the survival time of bacteria due to the inherent antimicrobial affinity for phosphate and S-thiols in the bacterial membranes being the Cu (II) a strong electron donors.[36] Cu-added in very small amounts films accelerated bacterial (e.g., *E. coli*) inactivation under natural sunlight, as recently reported.[37] Moreover, Cu positive ions contribute to the electrostatic attraction between the negative *E. coli* cell wall and the TiO_2–ZrO_2–Cu films.[18] Cu-ions left on the sputtered Cu-particles PES[18,38] surface during bacterial reduction are probably reduced to Cu^0 because both Ti^{4+}/Ti^{3+} and Zr^{4+}/Zr^{3+} couples have a standard hydrogen electrode (SHE) potential well above (more energetic) compared to the couple Cu^{2+}/Cu^0 0.34 V.[39] The Cu intragap states in very low concentrations (Table 2) have been very often invoked as precluding the recombination of the photogenerated electron/holes in the TiO_2.[40,41] The role of Cu would then be to promote the electron indirect transitions in the TiO_2 band gap leading to the significant shorter bacterial reduction kinetics. In Figure 1b, traces 3 and 4 show the slower bacterial inactivation on Cu-PES samples compared to TiO_2–ZrO_2–Cu samples. This points out the drastic increase on the bacterial inactivation kinetics when Cu was added compared to the TiO_2–ZrO_2 matrix.

Stereomicroscopy of *E. coli* on Stained Bacteria Samples. Figure 2 shows the live/dead *E. coli* bacteria by using the dye fluorochrome that enters the cell and stains the cytoplasma DNA only if the cell wall membranes are damaged showing an abnormal high permeability.[42] To test the time at which *E. coli* cells suffer destabilization/damage leading ultimately to cell dead (red dots indicate membrane damage), we incubated the cells on TiO_2–ZrO_2–Cu PES after irradiation in the cavity of the Suntest simulator for times up to 30 min. Figure 2a shows only green cells at zero time. But the loss of viability becomes more significant for samples irradiated at longer times. This increases the red dot density due to

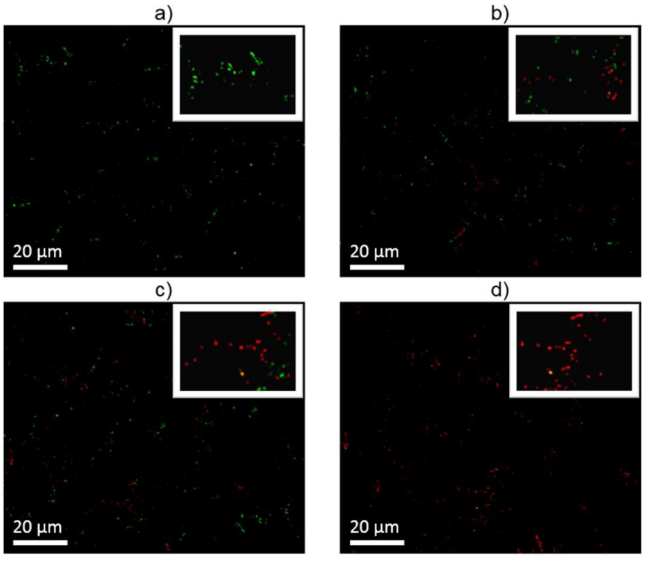

Figure 2. Live/dead bacteria on PES samples TiO_2–ZrO_2/Cu (8 min/10s): (a) time zero, (b) after 10 min, (c) after 20 min, and (d) after 30 min irradiation with low-intensity solar light (50 mW/cm^2).

DOI: 10.1021/acsami.5b02168
ACS Appl. Mater. Interfaces 2015, 7, 12832–12839

progressive membrane damage before cell death (Figure 2b–d).

Diffuse Reflectance Spectroscopy. Optical spectroscopy was used to measure the diffuse reflectance spectra in Figure 3a) for TiO_2, ZrO_2 and TiO_2–ZrO_2 transformed in Kubelka–Munk units. The DRS spectra of the 8 min sputtered films TiO_2 anatase is an indirect electron transition from the valence-band O 2p to the Ti 3d conduction band orbital in Figure 3a and is located at 380 nm corresponding to a band gap of 3.2 eV. Figure 3b presents the DRS spectroscopy of TiO_2–ZrO_2 sputtered for two different times. The spectra of the TiO_2 and ZrO_2 on PES coincide in Figure 3a is similar to the spectra reported in Figure 3b down to 380 nm. Additional peaks < 380 nm (Figure 3b,c) are due to UV polyester bands.[43] The interparticle electron transfer from ZrO_2 to TiO_2 has been reported to drive the chemical interaction between ZrO_2 and TiO_2 to form the Ti–O–Zr–bonds in the TiO_2–ZrO_2.[44−46] The broad-band shoulders in the TiO_2–ZrO_2 spectra at 320–340 nm in Figure 3a,b were assigned by Choi et al.[44] to the formation of the Zr–O–Ti bridges between TiO_2 and ZrO_2. The ZrO_2 (Figures 3a,b) shows an absorption edge at 245 nm.[45,46]

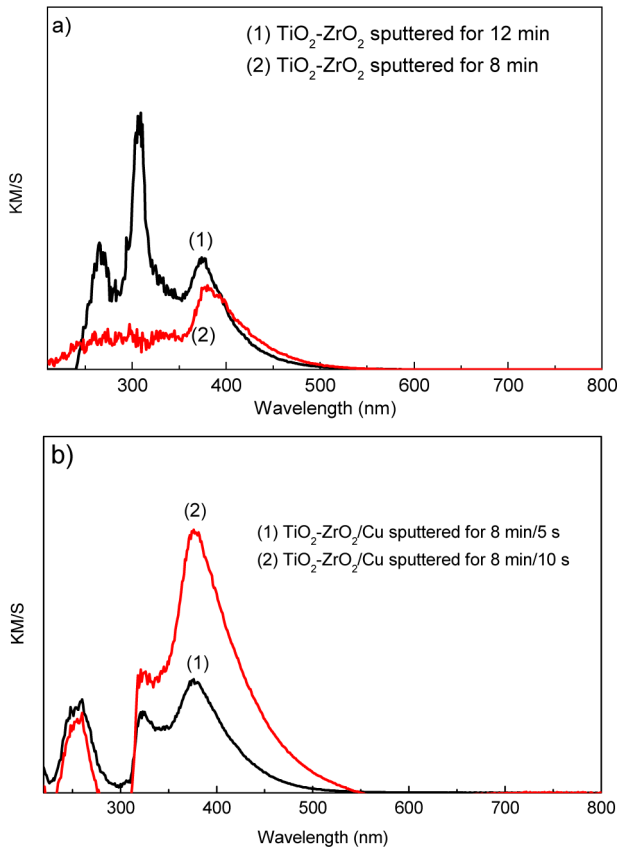

Figure 3. Diffuse reflectance spectroscopy of (a) TiO_2–ZrO_2 PES samples sputtered for 8 and 12 min and (b) TiO_2–ZrO_2/Cu PES samples sputtered for 8 min/5s and 8 min/10s.

Figure 3b shows that when Cu was added, the optical absorption due to Cu-plasmon(s) band[47] in the visible range was not observed and that no new bands were introduced in the TiO_2–ZrO_2 spectrum. Ionic Cu-doping sites on TiO_2 may undergo a one- or two-electron reduction potential of Cu(II) to Cu(I) or Cu^0 of 0.15 and 0.34 eV, in the TiO_2. The introduction of such energy levels leads to intragap states in the TiO_2 band gap red shifting the interfacial charge transfer and precluding the TiO_2 e^-/h^+ recombination.

Band Gap Determination of the Composites Sputtered Samples. The DRS spectra reported in Figure 3a,b were transformed in Kubelka–Munk units vs the spectral energy (eV) in Figure 4. The Tauc's plot[48] of $(F-(R)h\nu)^n$ against the energy axis is shown in Figure 4b. The optical band gap was estimated by extrapolating the linear part of the spectra vs the energy axis. The band gap energy levels found are shown in Figure 4c, trace 1) TiO_2–ZrO_2–Cu (8 min/10s) 2.26 eV, trace 2) TiO_2–ZrO_2–Cu (8 min/5s) 2.44 eV, trace 3) TiO_2–ZrO_2 12 min, 2.59 eV, trace 4) TiO_2–ZrO_2 8 min, 2.38 eV. Traces 3 and 4 show that the band gaps change with the sputtered concentrations of Ti and Zr. The band gaps estimated for TiO_2–ZrO_2 are narrower than the values for the TiO_2 and ZrO_2 semiconductors of 3.2 and 4.5 eV respectively.[9,32] Figure 4 also shows that only a marginal modification is introduced on the TiO_2–ZrO_2 band gap by the Cu.

X-ray Diffraction of TiO_2–ZrO_2 and TiO_2–ZrO_2–Cu Sputtered Films. Figure 5, traces 1 and 2, presents the XRD of TiO_2–ZrO_2 double oxide films diffractogram cosputtered at different times. Figure 5, trace 1, shows a decrease for the TiO_2 anatase peak and also for the ZrO_2 peak due to the addition of Cu 0.02% wt Cu/wt PES. The lack of a XRD signal for Cu is due to its very low atomic percentage concentration sputtered to decorate to the TiO_2–ZrO_2 network. Even the Cu-sputtering within seconds allows the Cu to penetrate in TiO_2–ZrO_2 to the TiO_2–ZrO_2 network.

The Cu addition to the TiO_2–ZrO_2 double oxide film has been investigated and reported already preventing the anatase to rutile transition.[15,41,49] The anatase phase is present in the TiO_2–ZrO_2 double oxide film cosputtered at 120–130 °C.[9,10] How the Cu- penetrates in the TiO_2–ZrO_2, interstitially or by substitution, is an open question. But Cu does not present any absorption band in the DRS spectrum, as shown in Figure 3a,b, and does not show any additional peaks in the XRD spectrogram in Figure 5. Moreover, the TiO_2–ZrO_2 XRD diffractogram in Figure 5 with and without Cu were observed to be similar.

X-ray Photoelectron Spectroscopy. Evidence by XPS shifts was found for the redox catalysis in the TiO_2–ZrO_2–Cu PES before and after bacterial inactivation. The shifts in binding energy (BE) of TiO_2 and ZrO_2 confirm the molecular level mixing in the composite network active in the photocatalysis. But evidence was also found for Cu redox processes during bacterial inactivation. The intensities of the Ti and Zr-peaks did change only upon Cu-sputtering, and this is indicative for the integrity of the TiO_2–ZrO_2 microstructure.

Figure 6a presents the deconvoluted peaks for the Ti 2p3/2 XPS envelope at time zero. Two well-resolved peaks with binding energies (BE) at 458.5 and 4.64 eV for the TiO_2 core XPS spectrum were detected and shown in Figure 6. This is the evidence for the presence of a single type of TiO_2 with an oxidation state of 4+. The signal for the BE of Ti–Zr was found at 460.1 and 457.5 eV. Evidence for the PES substrate binding to TiO_2 is shown by the Ti–C signal at 461.1 eV. The band energies in eV are assigned according to refs 50 and 51 and corrected for the electrostatic charging according to Shirley.[52] Figure 6b shows for samples after bacterial inactivation show the shift of the Ti–OH peak with respect to the same peak in Figure 6a (time zero) by 0.3 eV. Any shift >0.2 eV corresponds to a true change in an XPS spectrogram.[50] The shift noted for

DOI: 10.1021/acsami.5b02168
ACS Appl. Mater. Interfaces 2015, 7, 12832−12839

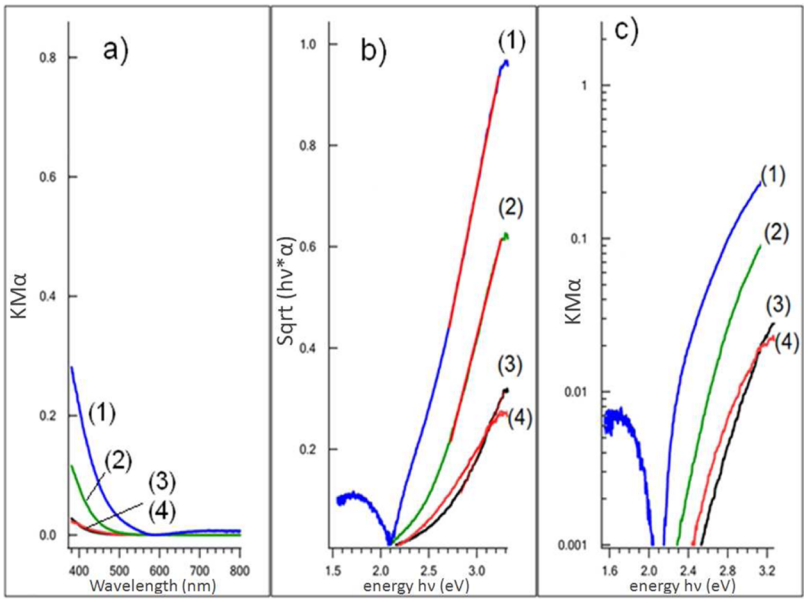

Figure 4. DRS spectra showing the indirect transition on the photocatalysts: (1) TiO_2–ZrO_2 sputtered on PES for 8 min followed by Cu(10s), (2) TiO_2–ZrO_2 sputtered on PES for 8 min followed by Cu(5s), (3) TiO_2–ZrO_2 sputtered on PES for 12 min, (4) TiO_2–ZrO_2 (sputtered on PES for 8 min). (a) Absorption in Kubelka–Munk units and (b and c) Tauc's equation to estimate band-gaps.

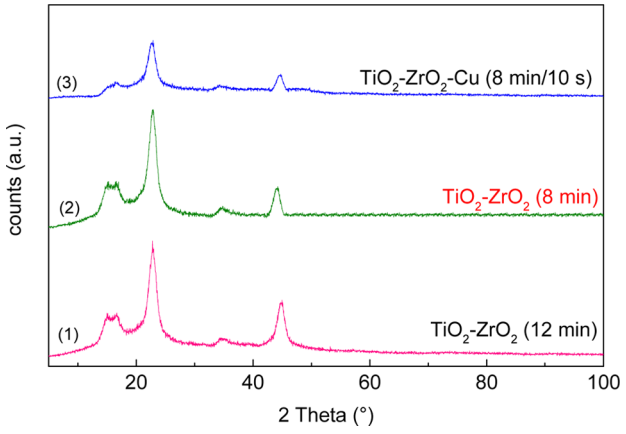

Figure 5. XRD spectrograms of (1) TiO_2–ZrO_2 PES samples cosputtered for 12 min, (2) TiO_2–ZrO_2 PES samples cosputtered for 8 min, and (3) TiO_2–ZrO_2–Cu PES samples cosputtered with TiO_2–ZrO_2 for 8 min followed by Cu-sputtering for 10 s.

the Ti–OH and TiO_2–Zr peaks suggests the TiO_2–ZrO_2 network undergoing redox reactions during bacterial inactivation.

Figure 6c for ZrO_2 shows the peak for Zr 3d5/2 at 182.2 eV at time zero. In Figure 6d, the Zr–Ti and $Zr(OH)_4$ band positions shift after bacterial inactivation. In separate experiments Cu-peaks were taken at time zero and after the bacterial inactivation (data not shown). At time zero, Cu(II) with a BE at 531.7 eV was observed. The peak of Cu(I)O at BE 529.5 eV appeared after bacterial reduction[18] implying Cu-reduction within the bacterial oxidation.

Bacterial Reduction Mechanism: Radical and Hole Trapping Experiments. Figure 7a shows the TiO_2–ZrO_2–Cu (8 min/10s) quenching of the highly oxidative radicals by selected quenchers during bacterial inactivation. The trapping of the radicals and holes photogenerated on TiO_2–ZrO_2–Cu PES were determined by selected scavengers, as shown in Figure 7a. SOD, DMSO, and EDTA-2Na were used to scavenge HO_2°/O_2^-, OH° radicals, and h^+, respectively, during the bacterial reduction of *E. coli*. In this way, we estimated the quantitative contribution of these radicals during the bacterial inactivation. Figure 7a shows that the bacterial inactivation was suppressed >80% by scavengers of HO_2°/O_2^-, OH° radicals and vbh^+ holes, in the order of h^+ > OH° > HO_2°/O_2^-. A simplified photocatalytic mechanism for bacterial reduction is suggested below. (Eqs 2 and 3 are taken from ref 53, and eq 4 is taken from ref 54.)

$$TiO_2 - ZrO_2 - Cu + h\nu \rightarrow h^+ + e^- \quad (1)$$

$$e^- + O_2 + H^+ \rightarrow HO_2^\circ \quad E_0 - 0.05\text{NHE} \quad (2)$$

$$e^- + O_2\text{ads} \rightarrow O_2^-\text{ads} \quad E_0 - 0.16\text{NHE} \quad (3)$$

$$h^+ + OH^-\text{ads} \rightarrow OH^\circ \quad E_0 - 1.90\text{NHE} \quad (4)$$

$$h^+ + H_2O\,\text{ads} \rightarrow OH\,\text{ads} + H^+ \quad (5)$$

In reaction 2 the HO_2° radical reacts at the physiological pH 6–8 in the form of O_2^- because $HO_2^\circ \rightarrow H^+ + O_2^-$ pK_a 4.8. The enhancement of the photocatalytic efficiency by TiO_2–ZrO_2 over both TiO_2 and ZrO_2 taken independently has been attributed to the enhanced generation of OH°-radicals.[35−43,45,46] The role of Cu accelerating the bacterial reduction by a factor of 3, as shown in Figure 1b, is possibly due to electron transfer from the valence band to the TiO_2 conduction band by Cu intragap states. The conduction band electrons will be shown in Figure 8 to react with the adsorbed oxygen, as shown in eqs 2 and 3, leading to highly oxidative radicals.

Figure 7a presents the evidence the important contribution of the OH°-radical to bacterial reduction. Next, the specific OH°-radical generation is reported in Figure 7b as a function of the TiO_2–ZrO_2–Cu (8 min/10s) irradiation time. The increase in the fluorescence intensity is a measure of the OH°-surface oxidative species generated by TiO_2–ZrO_2–Cu in

DOI: 10.1021/acsami.5b02168
ACS Appl. Mater. Interfaces 2015, 7, 12832−12839

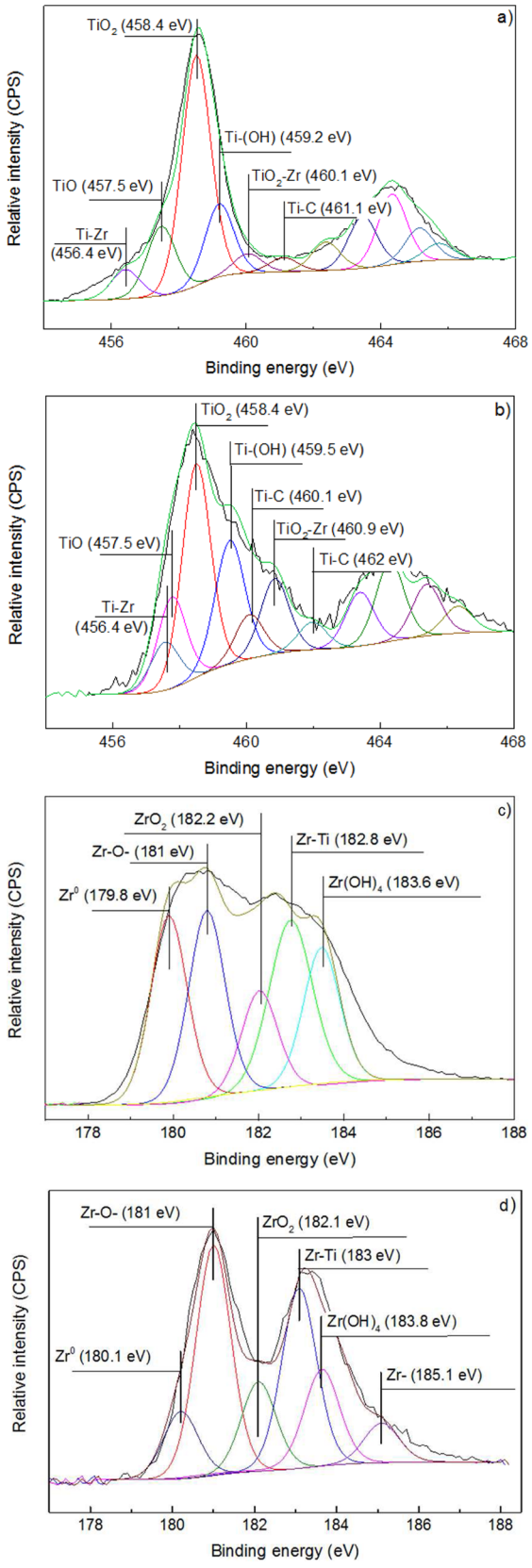

Figure 6. (a) Deconvoluted XPS envelope of the Ti 2p for TiO_2–ZrO_2/Cu PES sample sputtered for 8 min/10s before bacterial inactivation. (b) Deconvoluted XPS envelope of the Ti 2p for TiO_2–ZrO_2/Cu PES sample sputtered for 8 min/10s after bacterial inactivation. (c) Deconvoluted Z3d XPS envelope in TiO_2–ZrO_2/Cu PES sputtered samples for 8 min/10s before bacterial inactivation.

Figure 6. continued

(d) Deconvoluted Z3d XPS envelope in TiO_2–ZrO_2/Cu PES sputtered samples for 8 min/10s after bacterial inactivation.

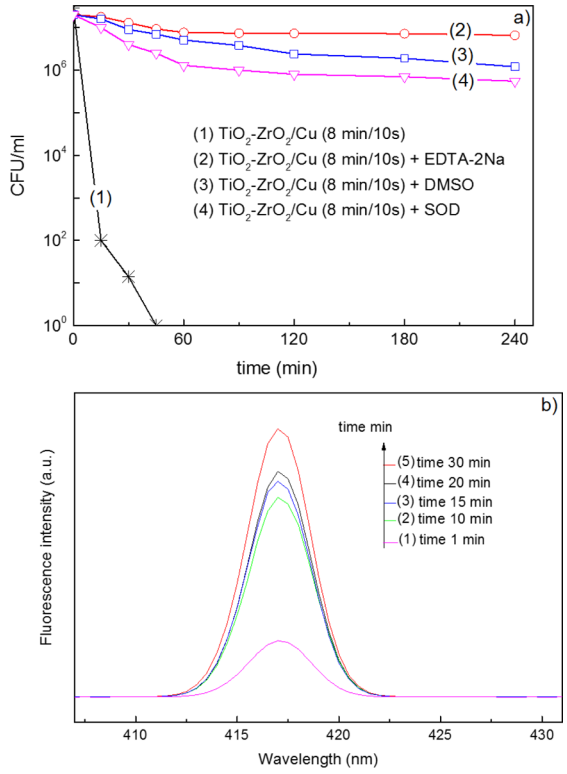

Figure 7. (a) *E. coli* inactivation on TiO_2–ZrO_2/Cu PES sputtered sample for 8 min/10s without and with the presence of various scavengers. For more details see text. (b) OH° production by a PES TiO_2–ZrO_2/Cu (8 min/10s) sample: after (1) 1, (2) 10, (3) 15, (4) 20, and (5) 30 min irradiation with low intensity solar light (50 mW/cm^2).

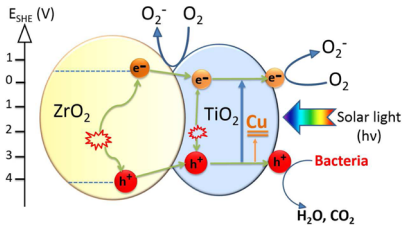

Figure 8. Interfacial charge transfer on TiO_2–ZrO_2 PES sample cosputtered for 8 min and TiO_2–ZrO_2/Cu PES cosputtered for 8 min/10s under low intensity solar light (50 mW/cm^2).

solution[31] increasing with irradiation time as shown in Figure 7b.

Interfacial Charge Transfer Mechanism in TiO_2–ZrO_2–Cu. Figure 8 shows the interfacial charge transfer mechanism for TiO_2–ZrO_2 and Cu doped TiO_2–ZrO_2. The TiO_2–ZrO_2–Cu presents more O_2 reduction points compared to TiO_2–ZrO_2 allowing the IFCT of Cu containing samples to achieve a higher yield in the O_2 reduction. The Cu intragap effect on the carrier mobility in TiO_2 will not be considered in detail because it is beyond the scope and objectives of this study and has been widely reported.[55−57] The transfer mechanism presented in Figure 8 follows the band model where the potential electronic

DOI: 10.1021/acsami.5b02168
ACS Appl. Mater. Interfaces 2015, 7, 12832−12839

positions are noted. A better charge separation is achieved by doping the TiO_2–ZrO_2 with Cu intragap sates accelerating bacterial inactivation (Figure 1b). The Cu-sputtered points act as intragap charge trap carriers and not as charge recombination centers due to the low Cu-amounts. The $Cu^{1+/2+}$ on the TiO_2–ZrO_2 surface may act as electron acceptor and enhance the removal of organics/bacteria because the one electron oxygen reduction $O_2 + H^+ + e^- \rightarrow HO_2^\circ$ proceeds at −0.05 V[53] and the $e^- + O_2 \rightarrow$ or O_2^- proceeds at −0.16 V. The Cu^{1+}-ion may reduce O_2 consuming electrons or oxidize to Cu^{2+} by the photogenerated TiO_2 holes[36].

CONCLUSIONS

This study reports the first account for the bacterial reduction inactivation of *E. coli* on TiO_2–ZrO_2–Cu–PES films. The effect of Cu doping to the TiO_2–ZrO_2 matrix is shown to drastically accelerate the bacterial inactivation kinetics. The band gap of TiO_2–ZrO_2–Cu was estimated and found to be narrower compared to the band gap of TiO_2–ZrO_2–Cu. This is important in practical application of these materials when exposed to sunlight irradiation. An IFCT mechanism is suggested for the photocatalysis via oxygen reduction. TiO_2–ZrO_2–Cu films seem to increase the oxygen reduction yield compared to TiO_2–ZrO_2, leading to a faster *E. coli* inactivation. The radicals intervening in the bacterial inactivation have been identified, and in the case of the OH°-radical, their increase reported as a function of the reaction time. Evidence for redox catalysis for some species in TiO_2 and ZrO_2 is presented within the bacterial reduction time by XPS measurements.

AUTHOR INFORMATION

Corresponding Author

*E-mail: john.kiwi@epfl.ch.

Notes

The authors declare no competing financial interest.

ACKNOWLEDGMENTS

We thank the EPFL, the Swiss National Science Foundation (SNF) Project (200021-143283/1) and the EC7th Limpid FP project (Grant No. 3101177) for financial support. We also thank the COST Actions and 1106 for interactive discussions during the course of this study.

REFERENCES

(1) Boucher, H.-W.; Talbot, G. H.; Bradley, J. S.; Edwards, J. E.; Gilbert, D.; Rice, L. B.; Scheld, M.; Spellberg, B.; Bartlett, J. Bad Bugs, No Drugs, No Escape. An Update from the Infectious Diseases Society of America. *Clin. Infect. Diseas* **2009**, *48*, 1–12.

(2) Pittet, D.; Tarara, D.; Wenzel, R. P. Nosocomial Bloodstream Infection in Critically Ill Patients. Excess Length of Stay, Extra Costs, and Atributable Mortality. *JAMA, J. Am. Med. Assoc.* **1994**, *271*, 1598–1601.

(3) Allegranzi, B.; Bagheri-Nejad, S.; Combescure, C.; Graafmans, W.; Attar, H.; Donaldson, L.; Pittet, D. Burden of Endemic Health-Care-Associated Infection in Developing Countries: Systematic Review and Meta-analysis. *Lancet* **2011**, *377*, 228–241.

(4) Plowman, R.; Graves, R.; Griffin, N.; Taylor, L. The Rate and Cost of Hospital-Acquired Infections Occurring in Patients Admitted to Selected Specialties of a District General Hospital in England and the National Burden Imposed. *J. Hosp. Infect.* **2001**, *47*, 198–209.

(5) Dance, S. The Role of Environmental Cleaning in the Control of Hospital Acquired Infections. *J. Hosp. Infect.* **2007**, *7*, 378–389.

(6) Kramer, I.; Schwebke, I.; Kampf, G. How Long Do Nosocomial Pathogens Persist in on Inanimate Surfaces? *BMC Infect. Diseases.* **2006**, *6*, 137–146.

(7) Foster, H.; Ditta, I.; Varghese, S.; Steele, A. Photocatalytic Disinfection using Titanium Dioxide: Spectrum of Antimicrobial Activity. *Appl. Microb. & Biotechnol.* **2011**, *90*, 1847–1868.

(8) TiO_2 Phtocatalysis, Fundamentals and Applications. BKC, Inc.: Tokyo, 2000.

(9) Fujishima, A.; Zhang, X.; Tryck, D. TiO_2 Photocatalysis and Related Surface Phenomena. *Surf. Sci. Rep.* **2008**, *63*, 515–582.

(10) Schneider, J.; Matsuoka, M.; Takeuchi, M.; Zhang, J.; Horiuchi, Y.; Anpo, M.; Bahnemann, D. Understanding TiO_2 Photocatalysis: Mechanisms and Materials. *Chem. Rev.* **2014**, *114*, 9919–9986.

(11) Fu, X.; Clark, L.; Yang, Q.; Anderson, M. Enhanced Photocatalytic Performance of Titania Based Binary Metal Oxides, TiO_2/SiO_2 and TiO_2/ZrO_2. *Environ. Sci. & Technol.* **1996**, *30*, 647–653.

(12) Zorn, M.; Tompkins, D.; Zeltner, W.; Anderson, M. Photocatalytic Oxidation of Acetone Vapor on TiO_2/ZrO_2 Thin Films. *Appl. Catal., B* **1999**, *23*, 1–8.

(13) Zhang, L.; Dillert, R.; Bahnemann, D.; Vormoor, M. Photo-induced Hydrophilicity and Self-Cleaning: Models and Reality. *Energy Environ. Sci.* **2012**, *5*, 7491–7507.

(14) T. Busko, T.; Dmytrenko, O.; Kulish, M.; Prylutskyy, Y.; Shokhovets, S.; Gobsch, G.; N. Vityuk, V.; Eremenko, A.; Tkach, V. Optical and Photocatalytic Properties of TiO_2 Films Modified with Oxides and Gold. *Materialwiss. Werkstofftech.* **2013**, *44*, 119–122.

(15) Kim, Ch; Jeong, H. Band Gap Tuning in Nanoporous TiO_2–ZrO_2 Hybrid Thin Films. *Bull. Korean Chem. Soc.* **2007**, *28*, 2333–2336.

(16) Borkow, G.; Gabbay, J. Copper an Ancient Remedy Returning to Fight Microbial, Fungal and Viral Infections. *Current. Chem. Biol.* **2009**, *3*, 272–278.

(17) Borkow, G.; Gabbay, J. Biocidal Textiles can Help Fight Nosocomial Infections. *Med. Hypothesis* **2008**, *70*, 990–994.

(18) Rtimi, S.; Baghriche, O.; Pulgarin, C.; Lavanchy, J.-C.; Kiwi, J. Growth of TiO_2/Cu by HIPIMS for Accelerated Bacterial Loss of Viability. *Surf. & Coat. Technol.* **2013**, *232*, 804–813.

(19) Baghriche, O.; Rtimi, S.; Pulgarin, C.; Sanjines, R.; Kiwi, J. Innovative TiO_2/Cu Surfaces Inactivating Bacteria <5 min under Low Intensity Visible/Actinic Light. *ACS Appl. Mater. Interfaces* **2012**, *4*, 5234–5240.

(20) Mills, A.; Hill, C.; Robertson, P. Overview of the Current ISO Tests for Photocatalytic Materials. *J. Photochem. Photobiol., A* **2012**, *237*, 7–23.

(21) Page, K.; Wilson, M.; Parkin, P. I. Antimicrobial Surfaces and their Potential in Reducing the Role of the Inanimate Environment in the Incidence of Hospital-Acquired Infections. *J. Mater. Chem.* **2009**, *19*, 3819–3831.

(22) Foster, H. A.; Sheel, P.; Sheel, W. D.; Evans, P.; Varghese, S.; Rutschke, N.; Yates, M. H. Antimicrobial Activity of Titatnia/Silver and Titania/Copper Films Prepared by CVD. *J. Photochem. Photobiol., A* **2010**, *216*, 283–289.

(23) Dunlop, M. S. P.; Sheeran, P. C.; Byrne, A. J. M.; McMahon, S. A.; Boyle, M. A.; McGuigan, G. K. Inactivation of Clinically Relevant Pathogens by Photocatalytic Coatings. *J. Photochem. Photobiol., A* **2010**, *216*, 303–3010.

(24) Yates, M. H.; Brook, A. L.; Ditta, B. I.; Evans, P.; Foster, H.; Sheel, A. W.; Steele, W. A. Photo-Induced Self–Cleaning and Biocidal Behviour of Titania and Copper Oxide Multilayers. *J. Photochem. Photobiol., A* **2008**, *197*, 197–2008.

(25) Kelly, P.; Li, H.; Benson, P.; Whitehead, K.; Verran, J.; Arnell, R.; Iordanova, I. Comparison of the Tribological and Antimicrobial Properties of CrN/Ag, ZrN/Ag, TiN/Ag, and TiN/Cu Nano-composite Coatings. *Surf. Coat. Technol.* **2010**, *205*, 1606–1610.

(26) Kelly, P.; Li, H.; Whitehead, K.; Verran, J.; Arnell, R.; Iordanova, I. A Study of the Antimicrobial and Tribological Properties of TiN/Ag Nanocomposite Coatings. *Surf. Coat. Technol.* **2009**, *204*, 1137–1141.

DOI: 10.1021/acsami.5b02168
ACS Appl. Mater. Interfaces 2015, 7, 12832–12839

(27) Bondarenko, O.; Katre, J. Toxicity of Ag, CuO and ZnO Nanoparticles Relevant Test to Mammalian Cell in Vitro: A Critical Review. *Arch. Toxicol.* **2013**, *87*, 1181−1200.
(28) Rtimi, S.; Pascu, M.; Sanjines, R.; Pulgarin, C.; Ben-Simon, M.; Houas, A.; Lavanchy, J-C.; Kiwi, J. ZrNO-Ag co-sputtered surfaces leading to E. coli inactivation under actinic light: Evidence for the Oligodynamic Effect. *Appl. Cat.* **2013**, *138*−*139*, 113−121.
(29) Mathews, W., Ed. *Epitaxial Growth*, J. Part B, Ch 4: Nucleation of Thin Films, Academic Press: New York, 1975, pp 382−486.
(30) Tauc, J.; Menth, A. States in the Gap. *J. Non-Cryst. Solids* **1972**, *8*−*10*, 569.
(31) Ishibashi, K.; Fujishima, A.; Watanabe, T.; Hashimoto, K. Quantum Yields of Active Oxidative Species Formed on TiO_2 Photocatalyst. *J. Photochem. Photobiol., A* **2000**, *134*, 139−142.
(32) Emeline, A.; Kataeva, G.; Litke, A.; Rudakova, A.; Riabchuk, V.; Serpone, N. Spectroscopic and Photoluminescence Studies of a Wide Band Gap Insulating Material: Powdered and Colloidal ZrO_2 Sols. *Langmuir* **1998**, *14*, 5011−5022.
(33) Fu, X.; Clark, L.; Yang, Q.; Anderson, M. Enhanced Photocatalytic Performance of Titania Based Binary Metal Oxides: TiO_2−SiO_2 and TiO_2−ZrO_2. *Environ. Sci. Technol.* **1996**, *30*, 647−683.
(34) Tian, G.; Kai, P.; Fu, H.; Jing, L.; Zhou, W. Enhanced Photocatalytic Activity of S-Doped TiO_2−ZrO_2 Nanoparticles under Visible Light Irradiation. *J. Hazard. Mater.* **2009**, *166*, 939−94.
(35) Shibata, K.; Kiyoura, T.; Kitagawa, J.; Sumiyoshi, T.; Tanabe, K. Acid Properties of Binary Mixed Oxides. *Bull. Chem. Soc. Jpn.* **1973**, *46*, 2985−2988.
(36) Qiu, X.; Miyaguchi, M.; Sunada, K.; Minoshima, M.; Liu, M.; Lu, Y.; Li, D.; Shimodaira, Y.; Hosogi, Y.; Kiroda, Y.; Hashimoto, K. Hybrid Cu_xO/TiO_2 Nanocomposites as Risk-Reduction Materials in Indoor Environments. *ACS Nano* **2012**, *6*, 1609−1618.
(37) Fisher, M.; Keane, D.; Fernández-Ibáñez, P.; Colreavy, J.; Hinder, S.; McGuigan; Pillai, S. Nitrogen and Copper Doped Solar Light Active TiO_2. Photocatalysts for Water Decontamination. *Appl. Catal., B* **2013**, *130*−*131*, 8−13.
(38) Sarakinos, K.; Alami, J.; Konstantinidis, S. High Power Pulsed Magnetron Sputtering: A Review on Scientific and Engineering State of the Art. *Surf. Coat. Technol.* **2010**, *204*, 1661−1684.
(39) *CRC Handbook of Chemistry and Physics, Electrochemical Series, D156*, CRC Press: Boca Raton FL, 1999.
(40) Morrison, S. R. *Electrochemistry at Semiconductor and Oxidized Surfaces*; Plenum Press: New York, 1982.
(41) Kiwi, J.; Morrison, C. Heterogeneous Photocatalyst Dynamic Charge Transfer in Doped Anatase Based Catalysts Powders With Enhanced Water Photocleavage Under Ultraviolet Irradiation. *J. Phys. Chem.* **1984**, *88*, 6146−6152.
(42) Gunawan, C.; Teoh, W.; Marquis, C.; Amal, R. Induced Antimicrobial Resistance to Nanosilver. *Small* **2013**, *9*, 3554−3560.
(43) French, H.; Rodríguez-Parada, J.; Yang, K.; Derryberry, R.; Lemon, M.; Brown, M.; Haeger, H.; Samuels, L.; Romano, R.; Richardson, R. Optical Properties of Materials for Concentrators & Photovoltaic System. *Sol. Energy Mater. Sol. Cells* **2011**, *95*, 3333−3342.
(44) Neppolian, B.; Wang, Q.; Yamashita, H.; Choi, H. Synthesis and Characterization of ZrO_2−TiO_2 Binary Oxide Semiconductor Nanoparticles: Application and Interparticle Electron Transfer Process. *Appl. Catal., A* **2007**, *333*, 264−271.
(45) Butler, E. C.; Davis, A. P. Photocatalytic Oxidation in Aqueous Titanium Dioxide Suspensions: The Influence of Dissolved Transition Metals. *J. Photochem. Photobiol., A* **1993**, *70*, 273−278.
(46) Jechachandran, L.; Narayandass, K. The Effect of Thickness of Titanium Nitride Coatings on Bacterial Adhesion. *Trends Biomater. Artif. Organs* **2010**, *24*, 90−93.
(47) Hardee, K.; Bard, A. Semiconductor Electrodes X. Photo-Electrochemical Behavior of Several Polycrystalline Metal Oxides Electrodes in Aqueous Solutions. *J. Electrochem. Soc.* **1978**, *124*, 215−224.
(48) Tauc, J. Optical Properties and Electronic Structure of Amorphous Ge and Si. *Mater. Res. Bull.* **1968**, *3*, 37−46.
(49) Dorian, A.; Hanaor, H.; Sorrell, C. Review of the Anatase to Rutile Phase Transformation. *J. Mater. Sci.* **2011**, *46*, 855−874.
(50) Wagner, C. D.; Riggs, M. W.; Davis, E. L.; Müllenberg, G. E., Eds., *Handbook of X-Ray Photoelectron Spectroscopy*; Perkin-Elmer Corp., Physical Electronics Division, Eden Prairie, MN, 1979.
(51) Nogier, J.; Delamar, M.; Ruiz, P.; Gratzel, M.; Thampi, R.; Kiwi, J. X-Ray Photoelectron Spectroscopy of TiO_2/V_2O_5. *Catal. Today* **1994**, *20*, 109−123.
(52) Shirley, A. D. Corrections of Electrostatic Charged Species in XPS-Spectroscopy. *Phys. Rev.* **1972**, *B5*, 4709−4716.
(53) Wardman, P. Reduction Potentials of One-Electron Couples Involving Free Radicals in Aqueous Solutions. *J. Phys. Chem. Ref. Data* **1989**, *18*, 1637−1755.
(54) Sulzberger, B.; Canonica, S.; Egli, T.; Giger, W.; Klausen, J.; von Gunten, U. Oxidative Transformations of Contaminants in Natural and Technical Systems. *Chimia* **1997**, *51*, 900−907.
(55) Bao, Z.; Lovinger, A.; Dodabalapur, A. Organic Field Effects Transistors with High Mobility Based on Copper Phthalocyanine. *Appl. Phys. Lett.* **1996**, *69*, 366−380.
(56) Kumar, G.; Gomanthi, D. Review on Modified TiO_2 Photocatalysis under UV/Visible Light: Selected Results and Related Mechanisms on Interfacial Charge Carrier Transfer Dynamics. *J. Phys. Chem. C* **2011**, *115*, 13211−13241.
(57) Akubuiro, E. C.; Verykios, X. E. Dopant-Induced Metal-Support Interactions: Influence on Chemisorptive Behavior. *J. Catal.* **1987**, *103*, 320−333.

DOI: 10.1021/acsami.5b02168
ACS Appl. Mater. Interfaces 2015, 7, 12832−12839